



The mineral weathering ability of *Collimonas pratensis* PMB3(1) involves a Malleobactin-mediated iron acquisition system

Laura Picard, Cédric Paris, Tiphaine Dhalleine, Emmanuelle Morin, Philippe Oger, Marie-Pierre M.-P. Turpault, Stéphane Uroz

► To cite this version:

Laura Picard, Cédric Paris, Tiphaine Dhalleine, Emmanuelle Morin, Philippe Oger, et al.. The mineral weathering ability of *Collimonas pratensis* PMB3(1) involves a Malleobactin-mediated iron acquisition system. *Environmental Microbiology*, 2022, 24 (2), pp. 784-802. 10.1111/1462-2920.15508 . hal-03194986

HAL Id: hal-03194986

<https://hal.science/hal-03194986>

Submitted on 9 Apr 2021

HAL is a multi-disciplinary open access archive for the deposit and dissemination of scientific research documents, whether they are published or not. The documents may come from teaching and research institutions in France or abroad, or from public or private research centers.

L'archive ouverte pluridisciplinaire **HAL**, est destinée au dépôt et à la diffusion de documents scientifiques de niveau recherche, publiés ou non, émanant des établissements d'enseignement et de recherche français ou étrangers, des laboratoires publics ou privés.

TITLE: The mineral weathering ability of *Collimonas pratensis* PMB3(1) involves a Malleobactin-mediated iron acquisition system

Running title: Mineral weathering role of Malleobactin

AUTHORS: Laura Picard^{1,2}, Cédric Paris^{3,4}, Tiphaine Dhalleine¹, Emmanuelle Morin¹, Philippe Oger⁵, Marie-Pierre Turpault², Stéphane Uroz^{1,2}

¹ Université de Lorraine, INRAE, UMR1136 « Interactions Arbres-Microorganismes », F-54280 Champenoux, France

² INRAE, UR1138 « Biogéochimie des Ecosystèmes Forestiers », F-54280 Champenoux, France

³ Université de Lorraine, EA 4367 « Laboratoire d'Ingénierie des Biomolécules », Ecole Nationale Supérieure d'Agronomie et des Industries Alimentaires (ENSAIA), F-54505 Vandœuvre-lès-Nancy, France

⁴ Plateau d'Analyse Structurale et Métabolomique (PASM) - SF4242 EFABA, F-54505 Vandœuvre-lès-Nancy, France

17 ⁵ Univ Lyon, INSA de Lyon, CNRS UMR 5240 « Microbiologie, Adaptation et
18 Pathogénie », F-69621, Villeurbanne France

19

20 * **Corresponding author:** Mailing address:

21 Université de Lorraine, INRAE, UMR 1136 “Interactions Arbres Microorganismes”,

22 54280 Champenoux, France. Phone: +33 (0)3 83 39 40 81, Fax: +33 (0)3 83 39 40

23 69. E-mail: stephane.uroz@inrae.fr.

24 SUMMARY

25 Mineral weathering (MW) by microorganisms is considered to occur through a
26 succession of molecular mechanisms based on acidification and chelation. While the
27 role of acidification is established, the role of siderophores is difficult to disentangle
28 from the effect of the acidification. We took advantage of the ability of strain
29 *Collimonas pratensis* PMB3(1) to weather minerals but not to produce organic acids
30 depending on the carbon source to address the role of siderophores in MW. We
31 identified a single non-ribosomal peptide synthetase (NRPS) responsible for
32 siderophore biosynthesis in the PMB3(1) genome. By combining iron-chelating
33 assays, targeted mutagenesis and chemical analyses (HPLC and LC-ESI-HRMS),
34 we identified the siderophore produced by strain PMB3(1) as malleobactin X and how
35 its production depends on the concentration of available iron. Comparison with the
36 genome sequences of other collimonads evidenced that malleobactin production
37 seems to be a relatively conserved functional trait, though some collimonads
38 harbored other siderophore synthesis systems. We also revealed by comparing the
39 wild-type strain and its mutant impaired in the production of malleobactin that the
40 ability to produce this siderophore is essential to allow the dissolution of hematite

41 under non-acidifying conditions. This study represents the first characterization of the
42 siderophore produced by collimonads and its role in mineral weathering.

43

44 **Key words:** *Collimonas pratensis* PMB3(1); mineral weathering; siderophore;
45 malleobactine; hematite

46

47

48

49

50

51 **Originality-Significance Statement**

52 Nutrient access is an essential process in nutrient-poor and non-amended
53 ecosystems. To deal with such conditions, plants have developed particular strategies to
54 adapt, noticeably through the selection in their rhizosphere of functional communities
55 effective at mobilizing the nutrients. Among them, bacteria have been shown to be
56 effective at mineral weathering (MW) and at promoting plant growth. Acidification and
57 chelation are considered as the main mechanisms used by MW bacteria. However,

our understanding of the molecular mechanisms and genes involved remains limited. While the role of acidification is established, the role of siderophores is difficult to disentangle from the effect of the acidification. In strain PMB3(1) of *Collimonas pratensis*, the production of organic acid by the central metabolism is dependent on the carbon source used for growth. Hence, it is one of the few bacterial models in which it is possible to decipher mineral weathering molecular mechanisms that are organic acid-independent. Strain PMB3(1) of *Collimonas pratensis* is a very effective MW bacterium, particularly adapted to oligotrophic environments and effective at promoting plant growth and at protecting plants against fungal pathogens. Mineral weathering has been proposed to be a functional trait of this genus, which molecular mechanisms have not yet been elucidated. The novel results obtained in this study through the combination of bioinformatics, chemical and phylogenetic analyses allowed us to identify and to characterized the siderophore produced by this model strain and to demonstrate the role of this iron acquisition system in mineral weathering. This study represents the first experimental demonstration of the siderophore produced by *Collimonas* (i.e., malleobactin). Our analyses allowed us to evidence the conservation of this iron acquisition system among collimonads and to

75 improve the siderophore prediction tools, especially to better discriminate ornibactin
76 and malleobactin. Our findings offer relevant informations for different fields of
77 research such as environmental genomics and chemistry, and soil sciences.

78

79 INTRODUCTION

80 Iron is an essential micronutrient for living organisms. It is involved in key cellular
81 processes such as DNA synthesis, respiration, photosynthesis or metabolism (Rout and Sahoo,
82 2015). Due to its oxidoreduction potential iron is used by several enzymes as energy source
83 (*i.e.* cytochrome subunit of enzymes or cofactors). Although this element is abundant in the
84 Earth crust, its bioavailability is strongly reduced in aerobic soils ranging from neutral to
85 basic pH, while in acidic soils such as in temperate forests, its bioavailability is higher.
86 However, it tends to decrease from the topsoil horizon to the deeper horizons due to the
87 precipitation of iron as iron oxi-hydroxides and its adsorption on different substrates such
88 as organic matter and primary minerals. In soils, the main sources of iron are the primary
89 minerals (*i.e.*, granite and other Fe-carrying minerals and rocks), the secondary
90 minerals such as iron oxi-hydroxides (*i.e.*, hematite, goethite) and the adsorbed
91 forms. However, most of those minerals dissolve at much slower rates than those required to
92 support plant and microbial growth (Lindsay, 1995). Consequently, iron access is subject to
93 important competitions between living organisms (Butaitė *et al.*, 2017).

94 The ability to mobilize iron from the different soil compartments (*i.e.*, minerals, rocks,
95 organic matter) has been reported for several plants, fungi, and bacteria. Noticeably, effective
96 iron mobilizing bacteria have been evidenced in the rhizosphere of various plants and in
97 different soils (Uroz *et al.*, 2009a). The presence of such bacteria and their relative enrichment
98 in the rhizosphere compared to the surrounding bulk soil suggest that these functional
99 communities are recruited in the root environment to make iron bioavailable for plant
100 nutrition. Among the effective iron mobilizing bacteria encountered in nutrient-poor forest

101 soils, bacteria belonging to the genus *Collimonas* have been described for their effectiveness
102 in mobilizing iron (Uroz *et al.*, 2009b, 2007; Leveau *et al.*, 2010). Although, collimonads
103 are considered as members of the rare biosphere in the soil (Leveau *et al.*, 2010),
104 they can be the dominant taxa in specific habitats such as in the mineralosphere
105 (Uroz *et al.*, 2015) or in the mycorrhizosphere (Lepleux *et al.*, 2012; Uroz *et al.*,
106 2012). Representatives of this genus have been isolated from various nutrient-poor
107 environments (*i.e.*, grass land, forests soil; (Uroz *et al.*, 2009b, 2014; Hoppener-
108 Ogawa *et al.*, 2008) and often in the close vicinity of fungi (De Boer, 2004; Uroz *et al.*,
109 2012). Some *Collimonas* species have been used as plant growth promoting agent
110 (*e.g.* tomatoes) to protect them against fungal pathogens (Kamilova *et al.*, 2007;
111 Senechkin *et al.*, 2013; Doan *et al.*, 2020) and to promote the growth of *Pinus*
112 *sylvestris* seedlings (Koele *et al.*, 2009). All these characteristics make this genus an
113 interesting plant growth-promoting (PGP) candidate.

114 The functional screening of *Collimonas* collections revealed that all the collimonads were
115 especially effective at weathering minerals compared to other genera. Among them,
116 *Collimonas pratensis* strain PMB3(1) appeared as the most effective (Uroz *et al.*, 2009b;
117 Picard *et al.*, 2020). This strain is able to solubilize inorganic phosphorous, mobilize iron and
118 dissolve minerals. At the molecular level, this high ability to weather mineral is explained by
119 the ability of the collimonads to produce protons *via* the direct oxidative pathway (Picard *et*

120 *al.*, 2021). Strain PMB3(1) is capable of strongly acidifying its environment when glucose is
121 used as sole carbon source and to produce high concentration of gluconic acid (Uroz *et al.*,
122 2009b; Picard *et al.*, 2021). In that respect, the glucose/methanol/choline (GMC)
123 oxidoreductase was identified as responsible for this acidification process in strain PMB3(1)
124 (Picard *et al.*, 2021). Other molecular mechanisms such as complexolysis may also play a role
125 in the dissolution of minerals (Uroz *et al.*, 2009a; Dong, 2010). Indeed, most of the bacteria
126 recruited in the rhizosphere are capable of producing siderophores. To date, different types of
127 siderophores have been reported and new chelating molecules are continuously discovered
128 (Hernandez *et al.*, 2004; Mathew *et al.*, 2014). Siderophores can impact directly (*i.e.*, surface
129 dissolution) or indirectly (*i.e.*, modification of the solution equilibrium) the mineral
130 weathering process, especially when carbon sources other than glucose are available (*i.e.*,
131 mannitol, trehalose) (Holmén and Casey, 1996; Kraemer, 2004; Parrello *et al.*, 2016; Perez *et*
132 *al.*, 2019).

133 In absence of acidification, the dissolution of minerals may occur through the action of
134 siderophores (Shirvani and Nourbakhsh, 2010), but no experimental study was done on
135 collimonads to functionally characterize the gene clusters involved and the type of
136 siderophore produced. The ability to chelate iron was evidenced for several *Collimonas*
137 strains (Uroz *et al.*, 2009b; Ballhausen *et al.*, 2016). More recently, bioinformatics analyses
138 identified genes encoding a potential Non-Ribosomal Peptide Synthetase (NRPS) in the
139 genomes of collimonads (*i.e.*, Ter6, Ter91, Ter331, Ter10, Ter282 and Ter291) and predicted
140 the production of ornibactin (Song *et al.*, 2015). In this context, the goals of this study were i)
141 to identify and chemically characterize the siderophore produced by the model *Collimonas*
142 *pratensis* strain PMB3(1), ii) to investigate how conserved the gene sequences were among
143 collimonads and related genera and iii) to determine the role of the siderophore in mineral
144 weathering. To do this, we combined bioinformatics, genomics, genetics, geochemistry and

145 functional bioassays to decipher the genes conferring the chelating and mineral weathering
146 abilities to strain PMB3(1) and other collimonads. The use of high-performance liquid
147 chromatography (HPLC) coupled to high-resolution and tandem mass spectrometry
148 (HRMS and MS/MS) allowed us to identify the siderophore produced as malleobactin X.

149

150 RESULTS

151 *Identification of a genomic region involved in siderophore production*

152 The CAS plate assay revealed that the model *Collimonas pratensis* strain
153 PMB3(1) produced chelating molecules as shown by the development of a yellow
154 halo around the colony (Fig. 1A). To identify the genomic region potentially involved
155 in the production of chelators in strain PMB3(1), an antiSMASH search was
156 performed on the genome sequence. Such analysis identified 11 regions encoding
157 putative polyketide synthases (PKS; n=2) or Non-Ribosomal Peptide Synthetases
158 (NRPS; n=9) with prediction or not of the final product (Table S2). Among the
159 potential NRPS, only one was predicted as encoding a siderophore. This region large
160 of 27.7 kb is characterized by 13 genes (Fig. 2; Table 2). Six genes are involved in
161 siderophore biogenesis. Among them the larger genes *mbaA* and *mbaB* encode

162 Non-ribosomal peptide synthetase (NRPS) composed of modules which including
163 domains (Condensation, Adenylation, Thiolation). In addition, the region is
164 characterized by 6 genes involved in siderophore transport and utilization and by one
165 gene encoding a sigma factor.

166

167 *Prediction of the siderophore structure*

168 To predict the structure of the siderophore, the two NRPS encoding genes (*mbaA*
169 NKI69295.1 and *mbaB* NKI69296.1) were submitted to NRPS prediction using three
170 different tools. All predictions identified four biosynthetic modules, three were
171 encoded by the *mbaA* gene and the last one by the *mbaB* gene. Modules are
172 composed of different domains: adenylation (A), thiolation (T), condensation (C) and
173 epimerization (E) following the schema (AT)-(CATE)-(CAT)-(CATC) for modules 1-2-
174 3-4 respectively. The NRPS prediction tools also proposed the amino acid
175 composition of the siderophore based on the Stachelhaus code (Stachelhaus *et al.*,
176 1999). For modules 2 and 3, the three NRPS prediction tools proposed the same
177 amino acids. Module 2 corresponds to a surfactin synthetase B (75 % identity) that
178 recruits an aspartate (Asp). Module 3 has 100 % identity with a pyoverdine synthetase

179 that recruits a serine (Ser). No consensus was obtained for modules 1 and 4. Indeed,
180 the signature sequence (DVETLGGISK or DVETLGGI) identified for module 1
181 indicated the recruitment of beta-hydroxy-tyrosine according to 'NRPS predictor 2' or
182 an ornithine according to 'NP.searcher'. For the amino acid recruited by the module
183 4, the signature sequence was DGEYTGGITK or DGEYTGGI. Such sequence is
184 predicted to recruit a leucine according to 'NRPS predictor 2' and 'NP.searcher', or
185 an ornithine according to 'PKS/NRPS analysis'. Altogether, our bioinformatics
186 analyses predicted a siderophore composed of four amino acids, the second being a
187 serine and the third an aspartate (X-Ser-Asp-X).

188

189 *Involvement of the mbaA gene in the production of siderophore*

190 To demonstrate the involvement of this NRPS encoding region in siderophore
191 synthesis, a *mbaA* mutant named Δ NRPS was constructed and tested using different
192 bioassays (*i.e.*, siderophore production, growth assay).

193 Regarding the ability to chelate iron, the WT strain of PMB3(1) was able to
194 mobilize iron in the CAS plate assay after 3 days. The yellow halo formed around the
195 colonies (WT colony diameter: 1.0 ± 0.1 cm) was about 1.5 ± 0.1 cm, while no halo

196 was observed for the Δ NRPS mutant strain (Δ NRPS colony diameter: 0.6 ± 0.1 cm)
197 (Fig. 1A). The production of chelating agent by the WT strain was also confirmed in
198 liquid CAS assay where the absorbance in absence of iron in the culture medium is
199 significantly decreased (OD at 655 nm = 0.053 ± 0.001) compared to the control.
200 Noticeably, for the WT strain, a siderophore activity was observed for iron
201 concentration ranging from 0 to 0.7 mg/l, while the production of chelator is inhibited
202 for greater values (iron concentration of 0.8 mg/l: OD at 655 nm = 0.372 ± 0.019 ;
203 $P < 0.05$) (Fig. 1B). Whatever the iron concentration, the Δ NRPS mutant did not
204 present a chelating activity (OD at 655 nm = 0.458 ± 0.005) (Fig. 1B).

205

206 *Impact of the mbaA mutation on growth*

207 To determine how the concentration of iron and the mutation of the *mbaA* gene
208 (Δ NRPS mutant) affect the growth of strain PMB3(1), were performed tests in
209 medium containing increasing concentrations of iron (*i.e.* 0.1; 0.2; 0.3; 0.5; 1.0 mg/l).
210 In this way, we demonstrated that the growth rate increased with increasing
211 concentrations of iron and that strain PMB3(1) and its Δ NRPS mutant presented the
212 same growth rate ($P > 0.05$) (Fig. S1). With 1 mg/l of iron, the growth rates of the

213 Δ NRPS mutant and WT strains without EDTA were ca $0.06 \pm 0.005 \text{ h}^{-1}$. However, in
214 presence of EDTA (10 mM), no growth was observed for the Δ NRPS mutant while
215 the growth of the WT strain was maintained, but its growth rate decreased to $0.01 \pm$
216 0.005 h^{-1} (Fig. 1C).

217

218 *Purification of the siderophore and chemical characterization*

219 To determine the structure of the synthesized siderophore, the supernatants of 3-
220 days old cultures in ABm devoid of iron of the WT strain (containing the siderophore),
221 the Δ NRPS mutant strain and the medium were analysed by HPLC and LC-ESI-MS
222 (or MS/MS).

223 The HPLC chromatograms of the WT, Δ NRPS mutant and medium supernatants
224 are presented in figure 3A. Such analysis evidenced a major peak with a retention
225 time (RT) of 1.2 min only present for the WT strain and absent from the two other
226 conditions. To investigate the potential presence of a siderophore activity associated
227 to this peak, the collected HPLC fractions were tested with the liquid CAS assay.
228 Both HPLC chromatogram and siderophore activity were overlaid and are presented
229 in figure 3B. Noticeably, the CAS assay revealed a strong reduction of the

absorbance ($OD_{655nm} = 0.055$) for the fractions corresponding to the peak present at RT = 1.2 min, matching with the yellow color observed with the CAS assay. This confirmed the presence of a chelating activity in the first peak. In addition, two other peaks were detected for the WT strain at 2.2 (peak 2) and 3.8 (peak 3) min RT (Fig. 3A). The liquid CAS assay revealed a decrease of absorbance ($OD_{655nm} = 0.110$ and 0.103 for peak 2 and 3, respectively; Fig. 3B) after 1h incubation, suggesting the presence of a chelating activity in the two peaks.

A deeper analysis was done by liquid chromatography coupled to positive ion-mode electrospray mass spectrometry (LC-ESI⁺-HRMS) on the first peak collected to perform the chemical characterization on a fraction which chelating activity was demonstrated. High resolution MS analysis revealed that the siderophore compound (S) has an exact mass of $M_s = 622.3069$ (monoprotonated ion seen at $m/z = 623.3069$) (Fig. 4A). This value is strictly similar to the mass of the malleobactin X (Fig. 4E). To confirm the malleobactin X structure, the siderophore was further analyzed by tandem mass spectrometry (MS/MS) and the major product ions (Fig. 4C) compared with theoretical fragments (Fig. 4D). Product ion at $m/z = 535.4$ (Fig. 4C; b₄) was attributed to the initial loss of C-terminal putrescine from the

precursor ion and that at $m/z = 517.4$ to additional dehydration (H_2O loss from $m/z = 535.4$). Product ion at $m/z = 465.3$ (also seen in its dehydrated form at $m/z = 447.4$) (Fig. 4C; y1) was attributed to the initial loss of N-terminal ornithine from the precursor ion. The breaking of the peptide bond between serine and ornithine gave rise to a product ion at $m/z = 377.2$ (also seen in its dehydrated form at $m/z = 359.2$) (Fig. 4C; b3) and another product ion at $m/z = 247.3$ (Fig. 4C; y3). The breaking between aspartate and serine gave rise to a product ion at $m/z = 334.3$ (Fig. 4C; y2).

An additional LC-ESI⁺-HRMS analysis was performed on the same fraction (collected at RT = 1.2 min), but previously incubated with iron (see details in *Ferrisiderophore preparation* section). As presented on Figure 4B, formation of the expected ferrisiderophore (FS) was confirmed through the clear observation of the ion at $m/z = 676.2191$ ($M_{FS (exp)} = 675.2191$). This experimental value is in full agreement with the complexation between iron (55.935 u for major isotope ^{56}Fe) and the triply deprotonated siderophore S ($622.3069 - 3 \times 1.008 = 619.2829$ u), leading to a theoretical mass $M_{FS (theo)} = 675.2179$ ($55.935 + 619.2829$). The presence of iron in the structure was also validated by the detection of the characteristic isotopic pattern detailed in Figure 4B, showing clearly the contributions of ^{54}Fe and ^{56}Fe isotopes

264 (m/z = 674.2246 and 676.2191, respectively). In addition, the relative intensities of
265 the ions at m/z = 677.2213 (28.8 %) and at m/z = 678.2236 (4.4 %) were found to be
266 in perfect accordance with the predicted isotopic distribution for malleobactin (Manura
267 and Manura, 2015). The MS/MS analysis conducted on the ferrisiderophore FS
268 (fragmentation of the ion at m/z = 676.2) revealed a product ion at m/z =
269 588.3 explained by the loss of C-terminal putrescine (dehydrated form also seen at
270 m/z = 570.2) (Fig. S2). A second intense ion at m/z = 606.2802 was also observed
271 on Figure 4B, in addition to that attributed to the ferrisiderophore FS (m/z =
272 676.2191).

273 The experimental masses found for the siderophore S (without incubation with
274 iron) and for the ferrisiderophore FS (after incubation of the siderophore with iron)
275 agree with the results previously obtained on *Burkholderia xenovorans* strain LB400
276 (Vargas-Straube *et al.*, 2016), allowing us to clearly identify the malleobactin X as the
277 siderophore produced by strain PMB3(1).

278

279 *Comparison with other Collimonas and related genera*

Our phylogenetic analysis revealed a good differentiation of the NRPS proteins according to the chemical structure of the siderophores (Fig. 5; green, ornibactin; red, malleobactin), the taxonomic belonging and the MbaA protein sequence. Beside the serobactin-related cluster, two clusters can be identified. The cluster 1 is supported by NRPS sequences (*i.e.*, Orbl homologues) assigned to *Burkholderia cepacia*, *B. cenocepacia* or *B. vietnamiensis* and is predicted to produce ornibactin. Noticeably, the production of ornibactin was experimentally demonstrated for three strains (*B. contaminans* MS14 (Deng *et al.*, 2017), *B. cenocepacia* K56-2 (Darling *et al.*, 1998), *B. cepacia* ATCC25416 (Meyer *et al.*, 1995)) of this cluster. The second cluster is composed of NRPS sequences (*i.e.*, MbaA homologues) assigned to *Burkholderia pseudomallei*, *B. mallei*, *B. thailandensis* and *Collimonas* and predicted to produce ornibactin or malleobactin. In this cluster, the production of malleobactin was experimentally demonstrated for three strains (*B. pseudmallei* K96243 (Alice *et al.*, 2006), *B. thailandensis* (Franke *et al.*, 2013), *B. xenovorans* LB400 (Vargas-Straube *et al.*, 2016)), while the production of ornibactin was only predicted. The strain PMB3(1) represents the fourth strains in this cluster which malleobactin production was experimentally demonstrated and the first collimonads. The strong proximity between the MbaA protein of the collimonads, the ability of strain PMB3(1) to produce malleobactin and the conserved ability to mobilize iron in collimonads suggest that all the collimonads considered synthesize malleobactin and not ornibactin as previously predicted (Fig. 5, green dotted circle; (Song *et al.*, 2015). Noticeably, the most distantly related sequence (38.25% of identity) to MbaA of

301 strain PMB3(1) is the NRPS protein responsible of the biosynthesis of serobactin in
302 *Herbaspirillum seropedicae* that is however the closest genus of *Collimonas* according to
303 taxonomy (Rosconi *et al.*, 2013).

304

305 *Siderophore involvement in hematite weathering*

306 To evaluate the potential involvement of the siderophore produced by *Collimonas*
307 strain PMB3(1) on mineral weathering, a hematite dissolution experiment was
308 performed (Fig. 6). To exclude an acidification effect, the experiment was done with
309 mannitol as sole carbon source, which was previously shown not to lead to the
310 acidification of the medium during growth (Uroz *et al.*, 2009b). After 7-days of
311 incubation, the iron released in solution from hematite as well as the pH were
312 measured, permitting to monitor the mineral weathering potential of the different
313 strains tested. In this experiment, no significant growth difference was observed
314 between the Δ NRPS mutant and the WT strains ($OD_{595nm} = 0.8 \pm 0.1$; $P < 0.05$),
315 though the WT strain released significantly more iron from the mineral (0.99 ± 0.19
316 mg/l; Fig. 6) than the Δ NRPS mutant strain or the non-inoculated controls (*i.e.* $0.01 \pm$
317 0.01 mg/l; $P < 0.05$). Noticeably, the pH of the medium remained stable at 6.2
318 whatever the treatment (inoculated with the WT strain, inoculated with the Δ NRPS

319 mutant strain and non-inoculated controls). In this sense, the CAS assay performed
320 on the supernatant for each condition demonstrated a siderophore activity (yellow
321 colour) only for the WT strain (Fig. 6).

322

323 DISCUSSION

324 The high effectiveness of *Collimonas pratensis* strain PMB3(1) to weather mineral
325 led us to investigate in more details the molecular mechanisms involved. In a
326 previous study, we showed that the mineral weathering effectiveness of this strain
327 was related to the carbon substrate used (*i.e.*, glucose, mannitol, trehalose,
328 gluconate; (Uroz *et al.*, 2009b)). In presence of glucose this strain strongly acidified the
329 medium and effectively weathers minerals, through the production of protons and
330 gluconic acids (Picard *et al.*, 2021). Noticeably, the strain PMB3(1) appeared also
331 capable of weathering minerals in presence of mannitol, a sugar highly produced by
332 mycorrhizal fungi and metabolized by this bacterial strain through a moderately-
333 acidifying pathway. The mineral weathering ability observed with mannitol suggests
334 the existence of alternative MW mechanisms such as iron acquisition systems. In this
335 study, we investigated the mechanisms by which this strain was able to mobilize iron

336 from artificial (*i.e.*, CAS) or natural iron complexes (*i.e.*, hematite). The *in silico*
337 analyses revealed that the genome of strain PMB3(1) harbors the *ftrABCD* system
338 (siderophore-independent iron uptake system; (Mathew *et al.*, 2014): [NKI69657.1-
339 NKI69654.1]), the bacterioferritin (iron storage protein; (Andrews, 1998): [NKI72009.1-
340 NKI72013.1]), the *fecIR* operon ((Braun *et al.*, 2003): [NKI68784.1-NKI68785.1]), and an
341 incomplete *hmu* operon ((Nienaber *et al.*, 2002); only *hmuU* [NKI72430.1] and *hmuV*
342 [NKI72429.1] were identified). In addition, an antiSMASH analysis identified a NRPS
343 cluster, predicted to synthesize a siderophore (*i.e.*, ornibactin). The presence in this
344 strain of all these iron acquisition systems suggests that it is quite adapted to the nutrient-poor
345 conditions occurring in the soil where it was isolated, but may also reflect the competition for
346 iron occurring in the mycorrhizosphere with other bacteria and fungi.

347

348 Although, strain PMB3(1) possesses all these putative iron acquisition systems, the knock-
349 out of a single gene of the NRPS cluster fully abolished its ability to mobilize iron as seen
350 using the CAS assay. These results suggest that the other iron acquisition systems play a
351 minor role in comparison to the production of siderophores or that they are important in other
352 processes such as the mobilization of intracellular iron reserves. The NRPS region detected
353 in strain PMB3(1) presents the classical structure found in other bacterial species
354 producing NRPS-dependent siderophores with the identification of genes involved in
355 siderophore biogenesis (including the 2 NRPS genes), in siderophore transport and

utilization (Fig. 2; (Esmaeel *et al.*, 2016, 2018; Butt and Thomas, 2017)). Noticeably, the *mbaA* and *mbaB* genes coding for siderophore production presented 36 % identity with genes *mbaA* and *mbaB* of *B. xenovorans* LB400, a strain capable of chelating iron and producing malleobactin (Vargas-Straube *et al.*, 2016). Different homologues of enzymes involved in N- and C-terminal modifications during siderophore production were also detected. These included *mbaH* which encodes a taurine dioxygenase TauD/F involved in the modifications on the N-terminal ornithine (Franke *et al.*, 2013), *mbaC* which encodes a L-ornithine 5-monooxygenase involved in the formation of a nitrogroup (Franke *et al.*, 2013) and *mbaE* encoding a N(5)-hydroxyornithine transformylase PvdF-type involved in modifications of the C-terminal ornithine (McMorran *et al.*, 2001; Vargas-Straube *et al.*, 2016). The *mbaI*, *J*, *L*, *N* and *D* genes involved in the ferrisiderophore complex recognition and transport were also identified (Butt and Thomas, 2017). In addition, the enzyme in charge of the reduction of the ferrisiderophore and of the release of Fe²⁺ and siderophore in the cytoplasm was identified as the *mbaK* gene encoding a siderophore-iron reductase FhuF (Matzanke *et al.*, 2004). The *mbaF* gene responsible of the siderophore expression and regulation was also identified as well as *mbaF*-dependent promoters

373 with specific -35 and -10 regions (TAAA/n(17)/CGTC) (Agnoli *et al.*, 2006; Thomas,
374 2007). Last, two genes (*iorA*, *iorB*) were identified at the end of the siderophore
375 biosynthesis region. They are predicted to encode two subunits of an aldehyde
376 dehydrogenase responsible of the formation of a carboxyl group. This function may
377 be responsible of modifications occurring after the synthesis of the siderophore.
378 However, a Δ lorB mutant presented no differences in siderophore mass (M_s =
379 622.3069) or in its chelating activity compared to the WT strain (data not shown). A
380 comparison with all the other available collimonads genomes revealed a good
381 conservation of the NRPS regions as well as of the *iorAB* genes. Indeed, the
382 complete NRPS region was found in nine of the 14 genomes and was absent from
383 the other five (*Collimonas sp.* OK242; *Collimonas sp.* OK307; *Collimonas sp.* OK607;
384 *Collimonas sp.* PA-H2 and *Collimonas arenae* Cal35). A more in-depth analysis of
385 the genomes of these collimonads revealed that some of them possessed genes
386 involved in the synthesis of other siderophores predicted to be myxochelin (41% of
387 homology for strains Cal35 and PA-H2) or staphylobactin (18% of homology for
388 strains OK242 and OK307). No siderophore region was detected for strain OK607.

389 These results suggest that malleobactin may not be the sole siderophore produced
390 by collimonads.

391

392 The combination of HPLC, fraction collect and mass spectrometry allowed us to
393 identify the siderophore produced by *Collimonas pratensis* strain PMB3(1) as
394 malleobactin. This hydroxamate type siderophore was reported for the first time to be
395 produced by *Pseudomonas pseudomallei* (reclassified as *Burkholderia pseudomallei*)
396 hence its name (Yang *et al.*, 1991). To date, different forms of malleobactin have been
397 discovered in different *Burkholderia* and *Paraburkholderia* species, be they members
398 or not of the *Burkholderia cepacia* complex (Bcc) (*i.e.* most pathogenic *Burkholderia*)
399 (Esmaeel *et al.*, 2016). In our study, the ESI-MS analysis revealed that the major
400 metabolite in the purified extract (*i.e.*, peak 1 with RT=1.2 min) had an exact mass of
401 $M_S = 622.3069$ and $m/z = 623.3069$ without iron and of $M_{FS} = 675.2191$ with iron (Fig.
402 4B). This compound effectively chelated iron as stated with the CAS assay. This
403 mass value obtained with iron corresponds perfectly with the mass of the
404 malleobactin previously identified in the strains *Burkholderia xenovorans* LB400
405 (Vargas-Straube *et al.*, 2016) and *Burkholderia thailandensis* (Franke *et al.*, 2013). In both

406 studies, the molecule detected was named malleobactin, but Vargas-Straube et al.
407 (2016) proposed the name malleobactin X and Franke et al. (2013) proposed
408 malleobactin B. The single difference between malleobactins B and X is the position
409 of an aldehyde group on the N-terminal ornithine. Such position was predicted by
410 Vargas-Straube et al., (2016) to be on the second nitrogen of the N-ter ornithine,
411 while Franke et al., (2013) determined it by NMR to be on the first nitrogen of the N-
412 ter ornithine. As the two molecules present the same properties (*i.e.*, mass,
413 fragmentation peaks, chelation ability) and the genome sequences are quite similar,
414 malleobactin B and X may correspond to the same molecule. For clarity in the text
415 we used the term malleobactin X. Finally, Vargas-Straube et al. (2016) also identified
416 another compound in the MS spectrum of the malleobactin produced by *B.*
417 *xenovorans* LB400 presenting a peak at $m/z = 606.4$ that they hypothesized to be a
418 fragment of the ferrisiderophore produced by a McLafferty rearrangement
419 (elimination of $\text{CH}_2\text{CHCH}_2\text{CH}_2\text{NH}_2$ corresponding to $[\text{M}_{\text{FS}}-70]^+$), but without the
420 demonstration of the presence of iron in this compound. For our strain PMB3(1) of
421 *Collimonas*, we detected a similar compound ($m/z = 606.2802$) in the MS spectrum of
422 the ferrisiderophore (*i.e.*, malleobactin + Fe). However, the isotopic profile of this ion

423 (m/z = 606.2802) did not present the characteristic iron signature, *i.e.* the clear
424 contributions of the two major iron isotopes ⁵⁴Fe and ⁵⁶Fe (Fig.S3). The absence of
425 iron signal indicates that the m/z = 606.2802 molecule is consequently not the result
426 of a Mc Lafferty rearrangement of the ferrisiderophore.

427

428 The chemical analyses granted us the possibility to authenticate two other minor
429 peaks (2 and 3; Fig. 3) in the purified extract, far less intense than the peak 1
430 corresponding to malleobactin (RT = 1.2 min). The absence of these two peaks in the
431 HPLC chromatogram of the extract of the Δ NRPS mutant (Fig. 3A) demonstrated that
432 the NRPS region we identified was responsible for the synthesis of (at least) the
433 three molecules (corresponding to the main peak 1 and the minor peaks 2 and 3).
434 Interestingly, the production of three different malleobactins by a single NRPS region
435 was also proposed for *Burkholderia pseudomallei* strain K96243, but the exact
436 structure and identity of these malleobactins were not reported (Alice *et al.*, 2006). In
437 the current work, we show that these two other molecules presented a lower
438 chelating activity than the main molecule we identified as malleobactin X. This is not
439 incongruent with these molecules being malleobactins. In fact, among the wide range

440 of malleobactins described (malleobactin A-H and X; (Franke *et al.*, 2015; Vargas-
441 Straube *et al.*, 2016), the affinity for iron strongly varies. Some of them (*i.e.*
442 malleobactin B, F and H) present such a low chelating activity compared to
443 malleobactin E that their real role in cell has been questioned (Franke *et al.*, 2015).
444 Thus diversity of malleobactin forms was proposed to result from the low specificity of
445 the adenylation domain A1 and A4 of the NRPS modules (Misiek *et al.*, 2011; Franke *et*
446 *al.*, 2015), but also from a spontaneous structural change (Franke *et al.*, 2013).
447 Noticeably, malleobactin B (similar to malleobactin X) was shown to undergo such a
448 structural change to other malleobactin forms (A, C or D) without any enzyme activity
449 (Franke *et al.*, 2013). Comparing the affinity for iron of these different forms revealed
450 that malleobactin A has a very low affinity. Based on the literature, our observations
451 suggest that the two minor peaks (2 and 3) represent alternate structures of the main
452 malleobactin detected in peak 1. However, due to their low concentration and low
453 affinity for iron, we were not able to determine their mass.

454

455 While the chemical characterization of the siderophore produced by strain
456 PMB3(1) allowed the identification of a malleobactin, the bioinformatic analyses done

457 on the NRPS genomic sequence (antiSMASH) predicted the production of ornibactin
458 (Stephan *et al.*, 1993). This discrepancy is mostly explained by the antiSMASH
459 database that does not contain malleobactin standard regions as few malleobactins
460 have been characterized at both chemical and genomic levels. The comparison of
461 the chemical structures of ornibactin and malleobactin reveals that they are strongly
462 similar (Alice *et al.*, 2006; Deng *et al.*, 2017). Indeed, the two siderophores differ only on
463 the N-terminal ornithine residue, where an aliphatic chain is present only on
464 ornibactin (Franke *et al.*, 2013). Such similarities suggest that the two siderophores are
465 encoded by very similar NRPS systems and that many predicted ornibactin-
466 producing bacteria may be malleobactin producers. To solve this issue of
467 identification, Esmaeel *et al.* (2016) proposed to add new criteria to differentiate the
468 NRPS-encoding ornibactin and malleobactin based on particular genes present or
469 absent in the NRPS clusters (Esmaeel *et al.*, 2016). They suggested that *orbK*-like and
470 *orbL*-like genes (encoding acetylases) are only present in ornibactin clusters,
471 whereas the presence of *mbaM* gene (encoding a protein of unknown function) was
472 only present in malleobactin clusters (Esmaeel *et al.*, 2016). However, the presence of
473 the *mbaM* gene was only highlighted for Burkholderiales (Butt and Thomas, 2017). In

474 our study, we do not detect a *mbaM* homologue in our model strain nor in the other
475 *Collimonas* strains or in *Burkholderia xenovorans* strain LB400, indicating that this
476 protein is not necessary for malleobactin production and is not a good marker of the
477 malleobactin cluster. The absence of the *orbK*-like and *orbL*-like genes are therefore
478 the most relevant for the identification of the malleobactin cluster.

479

480 Siderophores represent one of the main class of molecules reported to play an
481 important role in mineral weathering which are frequently detected in soil (Holmström
482 *et al.*, 2004). They are suspected to act directly on the mineral surfaces where they
483 form iron-siderophore complexes that are then transferred into the soil solution
484 (Kalinowski *et al.*, 2000; Kraemer, 2004). They may also indirectly act in MW by
485 chelating the iron released in solution, a phenomenon that modifies the equilibrium of
486 the surrounding solution and thus enhances mineral dissolution. While the effect of
487 pure molecules was clearly evidenced, the experiments done with bacteria producing
488 such molecules were less clear. Indeed, concomitantly to the production of
489 siderophores, many bacteria acidify their environment, making it difficult to
490 disentangle the relative effects of the acidification and the chelating molecules in the

491 mineral weathering process (Hersman *et al.*, 1995; Holmén and Casey, 1996; Maurice,
492 2000). Furthermore, several studies have shown a synergistic effect of siderophores
493 and acidifying molecules on mineral weathering (Reichard *et al.*, 2007; Dehner *et al.*,
494 2010; Lin *et al.*, 2018). Controlling the pH of the solution is therefore essential at
495 chemical, mineralogical and microbiological levels. First, it conditions the activity of
496 the siderophores. Deferrioxamine B, protochelin or rhizoferrin clearly showed
497 contrasted chelating activity with pH (Akafia *et al.*, 2014). Second, acidic conditions
498 allow a spontaneous dissolution of minerals (Brantley, 2008), which may release
499 significant quantities of iron in solution and consequently inhibit siderophore
500 production by bacteria. Indeed, the production of siderophore was shown to be
501 inhibited by iron concentrations ranging from 0.2 to 5 mg/l (Dave and Dubc, 2000; Deng
502 *et al.*, 2017) or in presence of Fe-bearing glasses (Perez *et al.*, 2019). In our study,
503 the production of malleobactin by strain PMB3(1) appeared inhibited from 0.8 mg/l of
504 iron in the solution, while the amount of iron released passively in solution from
505 hematite in our experimental conditions was below 0.1 mg/l. To exclude a potential
506 effect of acidification, our mineral weathering experiments were performed in a
507 buffered medium (constant pH = 6.2), devoid of iron and containing a carbon source

508 (*i.e.* mannitol), which does not permit an acidifying metabolism. Using this approach,
509 we were able to demonstrate for the first time that malleobactin production by
510 *Collimonas pratensis* strain PMB3(1) contribute to a significant increase of the
511 hematite dissolution as showed by comparing the WT and Δ NRPS mutant strains.
512 Together, our results suggest that depending on the availability of carbon substrates
513 (*i.e.*, glucose vs mannitol) and the nutrients (*i.e.*, quantity of iron in solution), strain
514 PMB3(1) may use high levels of organic acid such as gluconate and 2-keto-
515 gluconate or malleobactin to weather minerals and to scavenge iron from its
516 surrounding environment, two mechanisms which can act independently or in a
517 synergistic way (Picard *et al.*, 2021).

518

519 CONCLUSION

520 The combination of molecular and chemical methods allowed us to identify the
521 siderophore produced by *Collimonas pratensis* strain PMB3(1) as malleobactin X.
522 This is the first chemical and molecular characterization of a siderophore produced
523 by a collimonads as previous studies were only based on *in silico* analyses which
524 predicted that the siderophore produced by *Collimonas* was ornibactin (Song *et al.*,

2015). Malleobactin is a hydroxamate type siderophore characterized by a large diversity of structures that was previously reported in Burkholderiales and for several strains of *Burkholderia*. The conservation of the NRPS region among *Collimonas* species and the ability of the related strains to mobilize iron indicate that the production of malleobactin is a common trait among collimonads. It would be interesting to extend such analysis to a broader number of collimonads and neighboring genera. This study is also the first one demonstrating that malleobactin production is involved in mineral weathering. The use of a non-acidifying C source and of buffered conditions clearly proved the impact of malleobactin on the dissolution of hematite. Although malleobactin impacted hematite, a highly weatherable iron oxide, its impact on primary minerals present in soils such as phyllosilicate remains to be tested.

EXPERIMENTAL PROCEDURES

Bacterial strains and growth media

Bacterial strains, plasmids and primers are listed in Table 1. The model *Collimonas*
pratensis strain PMB3(1) studied here was isolated from oak (*Quercus petraea*)–
Scleroderma citrinum ectomycorrhizae sampled in the organo-mineral soil horizon
from the long term experimental forest site of Breuil-Chenue (Morvan region, France;
for sampling details see (Calvaruso *et al.*, 2007). This model strain was chosen for its
high mineral weathering effectiveness (Uroz *et al.*, 2009b, 2007). All strains were grown
at 25°C, except the strains of *Escherichia coli*, which were grown at 37°C. The media
used were Luria-Bertani (LB) and AB medium supplemented with mannitol (2 g/l final
concentration) as carbon source (ABm; (Chilton *et al.*, 1974). Gentamycin was added
to the media at 20 µg/ml (final concentration) when required.

551

552 *Preparation of bacterial inocula*

For each growth or functional assay presented below, the wild type (WT) strain
PMB3(1) and the mutant strain affected in its ability to mobilize iron (Δ NRPS) were
recovered from glycerol stock (-80 °C) and grown on ABm solid medium, amended
with gentamycin for the Δ NRPS mutant. After a 2-day incubation at 25 °C, one colony
of each strain was inoculated in liquid ABm medium (10 ml) and incubated for 2 days

558 at 25 °C under 200 rpm agitation. The cultures were then centrifuged at 8,000 g for
559 15 min at 10 °C and the pellet was washed twice with 5 ml of sterile Milli-Q water to
560 eliminate all culture medium and antibiotic traces. The pellet was recovered in 5 ml of
561 sterile Milli-Q water. To control the quantity of cells inoculated, the optical density
562 (OD) was measured at 590 nm and cell suspensions were adjusted at 0.90 ± 0.03 .

563

564 **Siderophore activity**

565 To determine the siderophore activity, the Chrome Azurol S (CAS) assay was
566 performed according to (Schwyn and Neilands, 1987) using the solid and liquid
567 versions. Both assays are based on the competition for iron between the CAS-Fe(III)
568 complex and siderophores. In absence of chelating agent, iron is associated to the
569 Chrome Azurol S and forms a blue complex. When a siderophore with a higher
570 affinity for iron is present, iron is released from the CAS-Fe(III) complex and the
571 colour of the CAS solution turns to yellow.

572 For the solid CAS assay, a volume of 5 µl of the bacterial inoculum of the WT or
573 the mutant strains were inoculated on CAS agar plates and incubated at 25 °C for 3

574 days. The presence of yellow halo was scored and its diameter as well as that of the
575 colony diameter was measured, to determine siderophore production and the growth.

576 For the liquid CAS assay, a volume of 100 μ l of the bacterial inoculum of the WT
577 or the mutant strains were inoculated in liquid ABm medium devoid of iron (10 ml)
578 and amended with gentamycin for the mutant strain. After 2-days incubation at 25 °C,
579 the cultures were centrifugated at 8,000 g for 15 min at 10 °C to recover the culture
580 supernatant. The supernatant was then filtered at 0.22 μ m (GHP Acrodisc 25 mm
581 syringe filter; PALL) and stored at -20 °C for further analyses. To evaluate the
582 presence of siderophore activity, 100 μ l of the filtered supernatant was added to
583 100 μ l of liquid CAS medium devoid of carbon source in a 96-well microplate. The
584 supernatant of non-inoculated medium was used as a negative control. After 1 hour
585 of incubation at room temperature in the dark, the absorbance was measured at OD
586 = 655 nm with a microplate reader (Bio-Rad, model iMark). The decrease of
587 absorbance corresponds to a change from blue color of the CAS complex to a yellow
588 color when a siderophore is present.

589

590 **Δ NRPS mutant construction**

591 Total DNA was extracted from the WT strain using the protocol of (Pospiech and
592 Neumann, 1995). To construct a targeted mutant of the gene *mbaA*, a portion of this
593 gene was amplified using the primers For-NRPS and Rev-NRPS (Table 1). These
594 primers amplified a region of ca. 2 kb of the *mbaA* gene characterized by the
595 presence of a natural *SmaI* site in its center. The purified PCR product was ligated
596 into the pGEM-T Easy plasmid (Promega) resulting in the plasmid pGEM-NRPS
597 (Table 1). The plasmid pGEM-NRPS was then digested with *SmaI* to introduce the
598 *SmaI*-digested gentamycin (Gm) resistance cassette from plasmid pUC1318,
599 resulting in the plasmid pGEM-NRPS::Gm. A fragment containing the *mbaA*::Gm
600 cassette was then obtained by *EcoRI* restriction and cloned in the plasmid pK19mob,
601 resulting in the pK19mob-NRPS::Gm plasmid. This construction was transferred to *E.*
602 *coli* S17.1 λ pir and then to strain PMB3(1) by bi-parental conjugation. Δ NRPS mutants
603 were recovered after 5 days of incubation at 25 °C on gentamycin-containing ABm
604 plates and organized in 96-microtiter plates. The transconjugants obtained were
605 verified by PCR with For-NRPS and Rev-NRPS primers, to differentiate the single
606 and double crossing-over events. Several single and double crossing-over mutants

607 were conserved. The experiments described in our study were done using a double
608 crossing-over mutant named Δ NRPS.

609

610 **Minimal concentration of iron inhibiting siderophore production**

611 To evaluate the concentration of iron inhibiting the siderophore production, the WT
612 strain and its Δ NRPS mutant were incubated with different concentrations of iron.

613 Briefly, in a 96-wells microplate, 10 μ l of calibrated suspension (described above) of

614 WT and Δ NRPS were inoculated in 180 μ l of ABm medium devoid of iron and 10 μ l of

615 a FeCl_3 solution. Different FeCl_3 solutions were prepared in Milli-Q water to obtain

616 final concentrations of iron ranging from 0 to 5 mg/l (0; 0.1; 0.2; 0.3; 0.5; 0.6; 0.7; 0.8;

617 0.9; 1.0; 1.5; 2.0; 2.5; 5.0 mg/l). A non-inoculated condition was performed as control.

618 After 3 days of incubation, the 96-wells microplate was centrifuged (1,100 g; 15 min)

619 and 100 μ l of supernatant were transferred to a new 96-wells microplate and mixed

620 with 100 μ l of CAS liquid solution (as described above). This solution was incubated

621 1 h in the dark before measuring the absorbance at 655 nm.

622

623 **Impact of iron concentration and iron competition on the growth of strain PMB3(1)**
624 **and its Δ NRPS mutant**

625 To determine how iron concentration affects the growth of the WT strain and its
626 Δ NRPS mutant, cultures were done in ABm medium devoid of iron and
627 supplemented or not with FeCl_3 (final concentration of iron: 0; 0.1; 0.2; 0.3; 0.5; 1.0
628 mg/l). A volume of 10 μl each of bacterial inoculum (*i.e.*, WT and mutant) was added
629 to 190 μl each of ABm medium described above. In addition, a competition assay
630 was done to determine how iron availability may affect the growth of strain PMB3(1)
631 and its Δ NRPS mutant. To do it, a strong chelator agent (*i.e.*, 10 mM of EDTA) was
632 added or not to the culture medium supplemented with 1 mg/l of iron. All samples
633 were tested in triplicate. The 96-well microplate was incubated at 25 °C on orbital
634 shaking during 3 days in a microplate reader (Tecan infinite M200 pro). The
635 absorbance was measured at OD = 600 nm every 3 hours. To evaluate the growth of
636 the strains, the slope of the exponential phase (*i.e.* growth rate) was calculated for
637 each condition and replicate.

638

639 **Chemical characterization of the siderophore**

640 *Siderophore production and purification*

641 To enable the chemical characterization of the siderophore(s) produced by strain
642 PMB3(1), cultures of 50 ml were done in iron-depleted ABm culture medium. The WT
643 strain and its Δ NRPS mutant were incubated 3 days at 25 °C under shaking (200
644 rpm). A non-inoculated condition was used as negative control. After this incubation
645 period, the cultures were centrifugated at 8,000 g for 15 min and the supernatant was
646 filtered at 0.22 μ m and stored at -20 °C for further analyses. The siderophore was
647 concentrated and purified using a Sep pack Vac 6cc tC18 Cartridges (Waters). The
648 column was first washed with 10 ml of 100 % methanol, then it was equilibrated with
649 10 ml of 0.01% trifluoroacetic acid (TFA) to acidify the column. Next, 25 ml of
650 supernatant was applied on the column. The siderophore was eluted with 5 ml of 10
651 % methanol solution (*i.e.* methanol / MQ water). The eluent was collected into 2 ml
652 eppendorf tubes and evaporated in a speedvacum system for 5h. The dried samples
653 were dissolved in 100 μ l of MQ water. The siderophore activity was tested using the
654 liquid CAS assay on the culture filtrate (0.22 μ m) as well as on the Sep pack purified
655 solution.

656

657 *Ferrisiderophore (FS) preparation*

658 A siderophore-containing extract was analyzed in the presence and in the absence
659 of an iron(III) acetate solution. Iron(III) solution was prepared with a 4-fold excess of
660 acetate relative to iron (25 mM) / acetate (100 mM). Iron(III) chloride (FeCl_3) was
661 initially dissolved in glacial acetic acid before dilution with water to desired volume
662 (pH=1.90) and finally double filtrated.

663 The formation of ferrisiderophore was carried out under non-inert atmosphere as
664 follows. Extract was first diluted 10 times (pH = 4.01) and pH was adjusted at pH 2.79
665 with 0.1 M HCl. Then, iron(III) acetate solution (25 mM, 100 μl) was added to 400 μl
666 of diluted extract to get the final reaction mixture (500 μl), at pH 2.46.

667 The control test was simply carried out by mixing 400 μl of 10-times diluted extract
668 with 100 μl of pure water, pH being adjusted under pH 3 with 0.1 M HCl.

669

670 *High Performance Liquid Chromatography (HPLC) analyses and fractionation*

671 The analysis was done on Sep pack treated supernatants coming from inoculated
672 (WT and ΔNRPS strains) or non-inoculated (control medium) media. Fifty microliters
673 of each supernatant were injected onto a Gemini C18 column (150 x 3.0 mm internal

674 diameter, 5 μ m particle size, Phenomenex) equilibrated with Milli-Q water with 0.01%
675 formic acid at 25 °C and connected to a Shimadzu Prominence HPLC system. A
676 gradient elution of Milli-Q water with 0.01% formic acid (buffer A) and acetonitrile with
677 0.01% formic acid (buffer B) for 40 min was used at a flow-rate of 1 ml/min and
678 detection was monitored with diode array UV-vis detector at 210 nm. The potential
679 peaks of interest were identified by comparing HPLC spectra and retention times
680 from the WT and Δ NRPS strains and the control medium samples.

681 To determine the siderophore activity of the peaks of interest, a fraction collect
682 was performed in 96-wells microplate using fraction collector system (FRC-10A
683 fraction collector system, Shimadzu). For each sample, fractions of 200 μ l were
684 recovered each 12 s using the same HPLC conditions described above. Fractions
685 were then evaporated in a speedvacuum system. Samples were suspended in 25 μ l of
686 CAS liquid assay diluted with 25 μ l of Milli-Q water and transferred in a new
687 microplate for absorbance measure at 655 nm.

688 To perform further mass spectrum analyses, the major peaks identified were
689 collected and the fractions combined to concentrate the metabolite of interest.

690

691 *Liquid chromatography coupled to high-resolution electrospray mass spectrometry*
692 *(LC-ESI-HRMS)*

693 Qualitative and semi-quantitative analysis of siderophores (S) and
694 ferrisiderophores (FS) was realized using a LC-ESI-HRMS method previously
695 described by (Paris *et al.*, 2021). The UHPLC-MS system (ThermoFisher Scientific,
696 San Jose, CA, USA) consists in a quaternary UltiMate 3000™ solvent delivery pump
697 connected to a photodiode array detector (PDA) and a LTQ-Orbitrap™ hybrid mass
698 spectrometer. Ten microliters of pre-purified HPLC extract were separated on a C18
699 Alltima reverse phase column (150 x 2.1 mm, 5 µm - Grace/Alltech, Darmstadt,
700 Germany) equipped with a C18 Alltima pre-column (7.5 x 2.1 mm, 5 µm) at 25 °C.
701 The flow rate was set at 0.2 ml/min and mobile phases consisted in water modified
702 with nonafluoropentanoic acid (NFPA) (5 mM) for A and pure methanol for B.
703 Compounds of interest were separated thanks to a program of 36 min, using a linear
704 gradient from 5 % to 98 % of B for 25 min.

705 Mass analysis was carried out in ESI positive ion mode (ESI⁺) and mass
706 spectrometry conditions were as follows: spray voltage was set at 4.5 kV; source
707 gases were set (in arbitrary units/min) for sheath gas, auxiliary gas and sweep gas at

708 40, 5 and 5, respectively; capillary temperature was set at 300°C; capillary voltage at
709 46 V; tube lens, split lens and front lens voltages at 112 V, - 70 V and - 6.25 V,
710 respectively.

711 Full scan MS spectra were performed at high resolution ($R=60000$ at m/z 400) on
712 the Orbitrap™ analyzer from 120 to 2000 m/z to obtain exact masses of siderophores
713 and ferrisiderophores on the HPLC purified peaks as well as on the total extract. MS²
714 full scan spectra were additionally realized for structural elucidation thanks to LTQ™
715 analyzer (Linear Trap Quadrupole). Raw data were processed using the
716 XCALIBUR™ software program (version 2.1, <http://www.thermoscientific.com>).

717

718 **Hematite weathering assay**

719 *Mineral description*

720 Hematite used as mineral in our study comes from a batch isolated in Brazil.
721 Hematite is an iron-oxide mineral of the oxides and hydroxides group. Iron oxides
722 (*i.e.*, hematite, goethite) occur, at least in small amounts, in nearly all soils (Dixon *et*
723 *al.*, 1989). Hematite is a widespread mineral occurring in a great variety of soils as a
724 result of the weathering of Fe-containing minerals (Dixon *et al.*, 1989). Igneous rocks

725 (*i.e.*, granite, trachyte, and rhyolite) can contain primary accessory grains of hematite.
726 This mineral was chosen for its high weatherability, its high content of iron and the
727 presence of hematite as secondary minerals in the experimental site where was
728 isolated the strain PMB3(1) (Calvaruso *et al.*, 2009). In this study, pure hematite
729 crystals were used (Fe_2O_3 pure at 99.3%) and containing in small amounts: 0.40%
730 TiO_2 , 0.18% SiO_2 , 0.16% Al_2O_3 , 0.10% MgO , 0.037% MnO .

731

732 *Mineral weathering assay*

733 The assay was performed in glass tubes containing 2 g/l of sterile hematite and
734 10 ml of ABm medium devoid of iron. Before introduction of hematite, the glass tubes
735 were rinsed with hydrochloric acid (HCl, 3.6 %) and MilliQ water. The tubes
736 containing the culture medium and hematite were then sterilised by autoclaving at
737 121°C. For the weathering assay, 100 μl of each bacterial inoculum (described
738 above; WT and ΔNRPS mutant strains) were used to inoculate the sterile glass
739 tubes. Non-inoculated media with and without hematite were used as controls. After
740 seven days of incubation at 25 °C (200 rpm), 200 μl of supernatant were sampled
741 and the OD at 595 nm was measured to determine bacterial growth. Then, 1 ml of

742 supernatant was centrifuged at 11,000 g for 15 min to remove bacterial cells.
743 Quantification of the iron released from hematite in the culture supernatant as well as
744 the pH were determined by adding 180 μ l of supernatant of each culture with 20 μ l of
745 ferrospectral or bromocresol green (1 g/l), respectively (Uroz *et al.*, 2007). The
746 absorbance of these suspensions was measured at 595 nm. The same culture
747 supernatant was also used to measure siderophore production with the liquid CAS
748 assay. The average values for three independent replicates for growth, iron
749 quantification, pH and siderophore production were used to determine the weathering
750 potential of the Δ NRPS mutant and the wild-type strains.

751

752 **Bioinformatic analyses**

753 *Genome properties gene localization and homology*

754 Genome analysis was performed using NCBI and MaGe (Vallenet, 2006). Homology
755 search analysis and alignment were performed with BLAST (BlastN and BlastP) (Altschul *et*
756 *al.*, 1990).

757 *In silico* search and identification of NRPS genes.

758 An *in silico* survey was done on the genome sequence of strain PMB3(1) to
759 identify the conserved domains of NRPS involved in siderophore production using

760 antiSMASH (Blin *et al.*, 2019). A combination of 3 tools based on the Stachelhaus
761 code of the adenylation domain was used to predict the amino acids recruited and the
762 potential structure of the siderophore produced (NRPS predictor (Rausch, 2005);
763 PKS/NRPS Analysis (Ansari *et al.*, 2004); NP.searcher (Li *et al.*, 2009)).

764

765 *Phylogenetic analysis on Collimonas genus*

766 As the MbaA protein is involved in the synthesis of the most variable part (*i.e.* N-
767 terminal part) of the siderophore, a phylogenetic analysis was performed on it (Franke
768 *et al.*, 2015). A total of 52 NRPS protein sequences were used to build a phylogenetic
769 PhyML tree with Seaview (version 4.5.4; (Gouy *et al.*, 2010)). These sequences were
770 chosen for their similarity to Orbl or MbaA proteins that are NRPS responsible of
771 ornibactin or malleobactin biosynthesis, respectively. Our analysis includes
772 sequences from *Collimonas* genera available online and other *Collimonas* related
773 genera (*i.e.* *Paraburkholderia*, *Burkholderia*, *Caballeronia*, *Herbaspirillum*) for which
774 the siderophores produced were predicted or experimentally demonstrated (Table
775 S1). As *Collimonas* is strongly related to *Herbaspirillum*, the NRPS protein involved in

776 serobactin production by *Herbaspirillum seropedicae* was included (Rosconi *et al.*,
777 2013).

778

779 **Statistical analyses.**

780 Statistical analyses were performed in R software. Data shown were means of at
781 least triplicates. Differences between sample's means were analysed by ANOVA and
782 TukeyHSD tests.

783

784 **Nucleotide sequence accession number.**

785 The whole-genome is available on NCBI under the accession no. WXXL01000000.

786

787 **ACKNOWLEDGMENTS**

788 This work was supported by grants from the EC2CO program of the CNRS to S.U.
789 and P.O. L.P. was also supported by a fellowship from the French Ministère de
790 l'Enseignement Supérieur, de la Recherche et de l'Innovation. The UMR1136 and
791 UR1138 are supported by the ANR through the Laboratory of Excellence Arbre
792 (ANR-11-LABX-0002-01).

793

794 REFERENCES

795 Agnoli, K., Lowe, C.A., Farmer, K.L., Husnain, S.I., and Thomas, M.S. (2006) The

796 ornibactin biosynthesis and transport genes of *Burkholderia cenocepacia* are

797 regulated by an extracytoplasmic function factor which is a part of the Fur

798 regulon. *J Bacteriol* **188**: 3631–3644.

799 Akafia, M.M., Harrington, J.M., Bargar, J.R., and Duckworth, O.W. (2014) Metal

800 oxyhydroxide dissolution as promoted by structurally diverse siderophores and

801 oxalate. *Geochim Cosmochim Acta* **141**: 258–269.

802 Alice, A.F., Lopez, C.S., Lowe, C.A., Ledesma, M.A., and Crosa, J.H. (2006) Genetic

803 and transcriptional analysis of the siderophore malleobactin biosynthesis and

804 transport genes in the human pathogen *Burkholderia pseudomallei* K96243. *J*

805 *Bacteriol* **188**: 1551–1566.

806 Altschul, S.F., Gish, W., Miller, W., Myers, E.W., and Lipman, D.J. (1990) Basic Local

807 Alignment Search Tool. *J Mol Biol* **215**: 403–410.

808 Andrews, S.C. (1998) *Advances in microbial physiology*, San Diego, Calif.; London:

809 Academic.

810 Ansari, Mohd.Z., Yadav, G., Gokhale, R.S., and Mohanty, D. (2004) NRPS-PKS: a
811 knowledge-based resource for analysis of NRPS/PKS megasynthases.
812 *Nucleic Acids Res* **32**: W405–W413.

813 Ballhausen, M.-B., Vandamme, P., and de Boer, W. (2016) Trait differentiation within
814 the fungus-feeding (mycophagous) bacterial genus *Collimonas*. *PLOS ONE*
815 **11**: e0157552.

816 Blin, K., Shaw, S., Steinke, K., Villebro, R., Ziemert, N., Lee, S.Y., et al. (2019)
817 antiSMASH 5.0: updates to the secondary metabolite genome mining pipeline.
818 *Nucleic Acids Res* **47**: W81–W87.

819 Brantley, S.L. (2008) Kinetics of Mineral Dissolution. In *Kinetics of Water-Rock*
820 *Interaction*. Brantley, S.L., Kubicki, J.D., and White, A.F. (eds). New York, NY:
821 Springer, pp. 151–210.

822 Braun, V., Mahren, S., and Ogierman, M. (2003) Regulation of the Fecl-type ECF
823 sigma factor by transmembrane signalling. *Curr Opin Microbiol* **6**: 173–180.

824 Butaitė, E., Baumgartner, M., Wyder, S., and Kümmerli, R. (2017) Siderophore
825 cheating and cheating resistance shape competition for iron in soil and
826 freshwater *Pseudomonas* communities. *Nat Commun* **8**: 414.

827 Butt, A.T. and Thomas, M.S. (2017) Iron acquisition mechanisms and their role in the
828 virulence of *Burkholderia* species. *Front Cell Infect Microbiol* **7**:.

829 Calvaruso, C., Mareschal, L., Turpault, M.-P., and Leclerc, E. (2009) Rapid clay
830 weathering in the rhizosphere of norway spruce and oak in an acid forest
831 ecosystem. *Soil Sci Soc Am J* **73**: 331–338.

832 Calvaruso, C., Turpault, M.-P., Leclerc, E., and Frey-Klett, P. (2007) Impact of
833 ectomycorrhizosphere on the functional diversity of soil bacterial and fungal
834 communities from a forest stand in relation to nutrient mobilization processes.
835 *Microb Ecol* **54**: 567–577.

836 Chilton, M.-D., Currier, T.C., Farrand, S.K., Bendich, A.J., Gordon, M.P., and Nester,
837 E.W. (1974) *Agrobacterium tumefaciens* DNA and PS8 bacteriophage DNA
838 not detected in crown gall tumors. *Proc Natl Acad Sci* **71**: 3672–3676.

839 Darling, P., Chan, M., Cox, A.D., and Sokol, P.A. (1998) Siderophore production by
840 cystic fibrosis isolates of *Burkholderia cepacia*. *Infect Immun* **66**: 874–877.

841 Dave, B.P. and Dubc, H.C. (2000) Regulation of siderophore production by iron
842 Fe(III) in certain fungi and fluorescent pseudomonads. *Indian J Exp Biol* **38**:
843 297–299.

844 De Boer, W. (2004) *Collimonas fungivorans* gen. nov., sp. nov., a chitinolytic soil
845 bacterium with the ability to grow on living fungal hyphae. *Int J Syst Evol*
846 *Microbiol* **54**: 857–864.

847 Dehner, C.A., Awaya, J.D., Maurice, P.A., and DuBois, J.L. (2010) Roles of
848 siderophores, oxalate, and ascorbate in mobilization of iron from hematite by
849 the aerobic bacterium *Pseudomonas mendocina*. *Appl Environ Microbiol* **76**:
850 2041–2048.

851 Deng, P., Foxfire, A., Xu, J., Baird, S.M., Jia, J., Delgado, K.H., et al. (2017) The
852 siderophore product ornibactin is required for the bactericidal activity of
853 *Burkholderia contaminans* MS14. *Appl Environ Microbiol* **83**:.

854 Dixon, J.B., Weed, S.B., and Dinauer, R.C. eds. (1989) Minerals in soil
855 environments, 2nd ed. Madison, Wis., USA: Soil Science Society of America.

856 Doan, H.K., Maharaj, N.N., Kelly, K.N., Miyao, E.M., Davis, R.M., and Leveau, J.H.J.
857 (2020) Antimycotal activity of *Collimonas* isolates and synergy-based
858 biological control of *Fusarium* wilt of tomato. *Phytobiomes J* **4**: 64–74.

859 Dong, H. (2010) Mineral-microbe interactions: a review. *Front Earth Sci China* **4**:
860 127–147.

861 Esmaeel, Q., Miotto, L., Rondeau, M., Leclère, V., Clément, C., Jacquard, C., et al.
862 (2018) *Paraburkholderia phytofirmans* PsJN-plants interaction: from
863 perception to the induced mechanisms. *Front Microbiol* **9**: 2093.

864 Esmaeel, Q., Pupin, M., Kieu, N.P., Chataigné, G., Béchet, M., Deravel, J., et al.
865 (2016) *Burkholderia* genome mining for nonribosomal peptide synthetases
866 reveals a great potential for novel siderophores and lipopeptides synthesis.
867 *MicrobiologyOpen* **5**: 512–526.

868 Franke, J., Ishida, K., and Hertweck, C. (2015) Plasticity of the malleobactin pathway
869 and its impact on siderophore action in human pathogenic bacteria. *Chem -*
870 *Eur J* **21**: 8010–8014.

871 Franke, J., Ishida, K., Ishida-Ito, M., and Hertweck, C. (2013) Nitro versus
872 hydroxamate in siderophores of pathogenic bacteria: effect of missing
873 hydroxylamine protection in malleobactin biosynthesis. *Angew Chem Int Ed*
874 **52**: 8271–8275.

875 Gouy, M., Guindon, S., and Gascuel, O. (2010) SeaView version 4: A multiplatform
876 graphical user interface for sequence alignment and phylogenetic tree
877 building. *Mol Biol Evol* **27**: 221–224.

878 Hernandez, M.E., Kappler, A., and Newman, D.K. (2004) Phenazines and other
 879 redox-active antibiotics promote microbial mineral reduction. *Appl*
 880 *Environnemental Microbiol* **70**: 8.

881 Hersman, L., Lloyd, T., and Sposito, G. (1995) Siderophore-promoted dissolution of
 882 hematite. *Geochim Cosmochim Acta* **59**: 3327–3330.

883 Holden, M.T.G., Seth-Smith, H.M.B., Crossman, L.C., Sebaihia, M., Bentley, S.D.,
 884 Cerdeño-Tárraga, A.M., et al. (2009) The genome of *Burkholderia*
 885 *cenocepacia* J2315, an epidemic pathogen of cystic fibrosis patients. *J*
 886 *Bacteriol* **191**: 261–277.

887 Holmén, B.A. and Casey, W.H. (1996) Hydroxamate ligands, surface chemistry, and
 888 the mechanism of ligand-promoted dissolution of goethite [α -FeOOH(s)].
 889 *Geochim Cosmochim Acta* **60**: 4403–4416.

890 Holmström, S.J.M., Lundström, U.S., Finlay, R.D., and van Hees, P.A.W. (2004)
 891 Siderophores in forest soil solution. *Biogeochemistry* **71**: 247–258.

892 Hoppener-Ogawa, S., de Boer, W., Leveau, J.H.J., van Veen, J.A., de Brandt, E.,
 893 Vanlaere, E., et al. (2008) *Collimonas arenae* sp. nov. and *Collimonas*

894 *pratensis* sp. nov., isolated from (semi-)natural grassland soils. *Int J Syst Evol*
895 *Microbiol* **58**: 414–419.

896 Kalinowski, B.E., Liermann, L.J., Brantley, S.L., Barnes, A., and Pantano, C.G.
897 (2000) X-ray photoelectron evidence for bacteria-enhanced dissolution of
898 hornblende. *Geochim Cosmochim Acta* **64**: 1331–1343.

899 Kamilova, F., Leveau, J.H.J., and Lugtenberg, B. (2007) *Collimonas fungivorans*, an
900 unpredicted in vitro but efficient in vivo biocontrol agent for the suppression of
901 tomato foot and root rot. *Environ Microbiol* **9**: 1597–1603.

902 Koele, N., Turpault, M.-P., Hildebrand, E.E., Uroz, S., and Frey-Klett, P. (2009)
903 Interactions between mycorrhizal fungi and mycorrhizosphere bacteria during
904 mineral weathering: Budget analysis and bacterial quantification. *Soil Biol*
905 *Biochem* **41**: 1935–1942.

906 Kraemer, S.M. (2004) Iron oxide dissolution and solubility in the presence of
907 siderophores. *Aquat Sci - Res Boundaries* **66**: 3–18.

908 Lepleux, C., Turpault, M.P., Oger, P., Frey-Klett, P., and Uroz, S. (2012) Correlation
909 of the abundance of betaproteobacteria on mineral surfaces with mineral
910 weathering in forest soils. *Appl Environ Microbiol* **78**: 7114–7119.

911 Leveau, J.H.J., Uroz, S., and de Boer, W. (2010) The bacterial genus *Collimonas* :
 912 mycophagy, weathering and other adaptive solutions to life in oligotrophic soil
 913 environments. *Environ Microbiol* **12**: 281–292.

914 Li, M.H., Ung, P.M., Zajkowski, J., Garneau-Tsodikova, S., and Sherman, D.H.
 915 (2009) Automated genome mining for natural products. *BMC Bioinformatics*
 916 **10**: 185.

917 Lin, Q., Wang, Y., Yang, X., Ruan, D., Wang, S., Wei, X., and Qiu, R. (2018) Effect of
 918 low-molecular-weight organic acids on hematite dissolution promoted by
 919 desferrioxamine B. *Environ Sci Pollut Res* **25**: 163–173.

920 Lindsay, W.L. (1995) Chemical reactions in soils that affect iron availability to plants.
 921 A quantitative approach. In *Iron Nutrition in Soils and Plants*. Abadía, J. (ed).
 922 Dordrecht: Springer Netherlands, pp. 7–14.

923 Manura, J.J. and Manura, D.J. (2015) Isotope Distribution Calculator and Mass Spec
 924 Plotter, Scientific Instrument Services (SIS).

925 Mathew, A., Eberl, L., and Carlier, A.L. (2014) A novel siderophore-independent
 926 strategy of iron uptake in the genus *Burkholderia*: Siderophore-independent
 927 iron uptake in *Burkholderia*. *Mol Microbiol* **91**: 805–820.

928 Matzanke, B.F., Anemüller, S., Schünemann, V., Trautwein, A.X., and Hantke, K.
 929 (2004) FhuF, part of a siderophore-reductase system †. *Biochemistry* **43**:
 930 1386–1392.

931 Maurice, P.A. (2000) Dissolution of Al-substituted goethites by an aerobic
 932 *Pseudomonas mendocina* var. bacteria. *Geochim Cosmochim Acta* **64**: 1363–
 933 1374.

934 McMorran, B.J., Sullivan, K., and Lamont, I.L. (2001) Involvement of a transformylase
 935 enzyme in siderophore synthesis in *Pseudomonas aeruginosa*. *Microbiology*
 936 1517–1524.

937 Meyer, J.-M., Van Van, T., Stintzi, A., Berge, O., and Winkelmann, G. (1995)
 938 Ornibactin production and transport properties in strains of *Burkholderia*
 939 *vietnamiensis* and *Burkholderia cepacia* (formerly *Pseudomonas cepacia*).
 940 *Biometals* **8**: 309–317.

941 Misiek, M., Braesel, J., and Hoffmeister, D. (2011) Characterisation of the ArmA
 942 adenylation domain implies a more diverse secondary metabolism in the
 943 genus *Armillaria*. *Fungal Biol* **115**: 775–781.

944 Nienaber, A., Hennecke, H., and Fischer, H.-M. (2002) Discovery of a haem uptake
 945 system in the soil bacterium *Bradyrhizobium japonicum*: Haem uptake system
 946 in *B. japonicum*. *Mol Microbiol* **41**: 787–800.

947 Paris, C., Selmeczi, K., Ebel, B., Stefan, L., Csire, G., Cakir-Kiefer, C., et al. (2021)
 948 Metabolomics approach based on LC-HRMS for the fast screening of iron(II)-
 949 chelating peptides in protein hydrolysates. *Anal Bioanal Chem*.

950 Parrello, D., Zegeye, A., Mustin, C., and Billard, P. (2016) Siderophore-mediated iron
 951 dissolution from nontronites is controlled by mineral cristallochemistry. *Front*
 952 *Microbiol* **7**:423.

953 Perez, A., Rossano, S., Trcera, N., Verney-Carron, A., Rommevaux, C., Fourdrin, C.,
 954 ... & Guyot, F. (2019). Direct and indirect impact of the bacterial strain
 955 *Pseudomonas aeruginosa* on the dissolution of synthetic Fe (III)-and Fe (II)-
 956 bearing basaltic glasses. *Chemical Geol*, 523: 9-18.

957 Picard, L., Oger, P., Turpault, M.-P., and Uroz, S. (2020) Draft genome sequence of
 958 *Collimonas pratensis* strain PMB3(1), an effective mineral-weathering and
 959 chitin-hydrolyzing bacterial strain. *Microbiol Resour Announc* **9**: e00601-20,
 960 /mra/9/37/MRA.00601-20.atom.

961 Picard, L., Turpault, M.-P., Oger, P.M., and Uroz, S. (2021) Identification of a novel
 962 type of glucose dehydrogenase involved in the mineral weathering ability of
 963 *Collimonas pratensis* strain PMB3(1). *FEMS Microbiol Ecol* fiae232.
 964 Pospiech, A. and Neumann, B. (1995) A versatile quick-prep of genomic DNA from
 965 gram-positive bacteria. *Trends Genet TIG* 11: 217–218.
 966 Rausch, C. (2005) Specificity prediction of adenylation domains in nonribosomal
 967 peptide synthetases (NRPS) using transductive support vector machines
 968 (TSVMs). *Nucleic Acids Res* 33: 5799–5808.
 969 Reichard, P.U., Kretzschmar, R., and Kraemer, S.M. (2007) Dissolution mechanisms
 970 of goethite in the presence of siderophores and organic acids. *Geochim*
 971 *Cosmochim Acta* 71: 5635–5650.
 972 Rosconi, F., Davyt, D., Martínez, V., Martínez, M., Abin-Carriquiry, J.A., Zane, H., et
 973 al. (2013) Identification and structural characterization of serobactins, a suite
 974 of lipopeptide siderophores produced by the grass endophyte *Herbaspirillum*
 975 *seropedicae*: Siderophores of *Herbaspirillum seropedicae*. *Environ Microbiol*
 976 15: 916–927.

- 977 Rout, G.R. and Sahoo, S. (2015) Role of iron in plant growth and metabolism. *Rev*
978 *Agric Sci* **3**: 1–24.
- 979 Schwager, S., Agnoli, K., Köthe, M., Feldmann, F., Givskov, M., Carlier, A., and
980 Eberl, L. (2013) Identification of *Burkholderia cenocepacia* strain H111
981 virulence factors using nonmammalian infection hosts. *Infect Immun* **81**: 143–
982 153.
- 983 Schwyn, B. and Neilands, J.B. (1987) Universal chemical assay for the detection and
984 determination of siderophores. *Anal Biochem* **160**: 47–56.
- 985 Senechkin, I.V., van Overbeek, L.S., Er, H.L., de Vos, O., and van Bruggen, A.H.C.
986 (2013) Interaction of *Collimonas* strain IS343 with *Rhizoctonia solani* at low
987 carbon availability *in vitro* and in soil. *Eur J Plant Pathol* **136**: 789–802.
- 988 Shirvani, M. and Nourbakhsh, F. (2010) Desferrioxamine-B adsorption to and iron
989 dissolution from palygorskite and sepiolite. *Appl Clay Sci* **48**: 393–397.
- 990 Song, C., Schmidt, R., de Jager, V., Krzyzanowska, D., Jongedijk, E., Cankar, K., et
991 al. (2015) Exploring the genomic traits of fungus-feeding bacterial genus
992 *Collimonas*. *BMC Genomics* **16**: 1103–1120.

- 993 Stachelhaus, T., Mootz, H.D., and Marahiel, M.A. (1999) The specificity-conferring
 994 code of adenylation domains in nonribosomal peptide synthetases. *Chem Biol*
 995 **6**: 493–505.
- 996 Stephan, H., Freund, S., Beck, W., Jung, G., Meyer, J.-M., and Winkelmann, G.
 997 (1993) Ornibactins? A new family of siderophores from *Pseudomonas*.
 998 *Biometals* **6**: 93–100.
- 999 Thomas, M.S. (2007) Iron acquisition mechanisms of the *Burkholderia cepacia*
 1000 complex. *BioMetals* **20**: 431–452.
- 1001 Uroz, S., Calvaruso, C., Turpault, M.-P., and Frey-Klett, P. (2009a) Mineral
 1002 weathering by bacteria: ecology, actors and mechanisms. *Trends Microbiol*
 1003 **17**: 378–387.
- 1004 Uroz, S., Calvaruso, C., Turpault, M.-P., Pierrat, J.C., Mustin, C., and Frey-Klett, P.
 1005 (2007) Effect of the mycorrhizosphere on the genotypic and metabolic
 1006 diversity of the bacterial communities Involved in mineral weathering in a
 1007 forest soil. *Appl Environ Microbiol* **73**: 3019–3027.
- 1008 Uroz, S., Calvaruso, C., Turpault, M.-P., Sarniguet, A., de Boer, W., Leveau, J.H.J.,
 1009 and Frey-Klett, P. (2009b) Efficient mineral weathering is a distinctive

1010 functional trait of the bacterial genus *Collimonas*. *Soil Biol Biochem* **41**: 2178–

1011 2186.

1012 Uroz, S., Kelly, L.C., Turpault, M.-P., Lepleux, C., and Frey-Klett, P. (2015) The

1013 mineralosphere concept: mineralogical control of the distribution and function

1014 of mineral-associated bacterial communities. *Trends Microbiol* **23**: 751–762.

1015 Uroz, S., Oger, P., Morin, E., and Frey-Klett, P. (2012) Distinct

1016 ectomycorrhizospheres share similar bacterial communities as revealed by

1017 pyrosequencing-based analysis of 16S rRNA genes. *Appl Environ Microbiol*

1018 **78**: 3020–3024.

1019 Uroz, S., Tech, J.J., Sawaya, N.A., Frey-Klett, P., and Leveau, J.H.J. (2014)

1020 Structure and function of bacterial communities in ageing soils: Insights from

1021 the Mendocino ecological staircase. *Soil Biol Biochem* **69**: 265–274.

1022 Vallenet, D. (2006) MaGe: a microbial genome annotation system supported by

1023 synteny results. *Nucleic Acids Res* **34**: 53–65.

1024 Vargas-Straube, M.J., Cámara, B., Tello, M., Montero-Silva, F., Cárdenas, F., and

1025 Seeger, M. (2016) Genetic and functional analysis of the biosynthesis of a

1026 Non-Ribosomal Peptide Siderophore in *Burkholderia xenovorans* LB400.

1027 *PLOS ONE* 11: e0151273.

1028 Yang, H.M., Chaowagul, W., and Sokol, P.A. (1991) Siderophore production by

1029 *Pseudomonas pseudomallei*. *Infect Immun* 59: 776–780.

1030

1031

1032

1034 **Table 1: List of bacterial strains, constructions and primers used in this study**

Strains, plasmids or primers	Characteristics	R e f e r e n c e
------------------------------	-----------------	---

S

U

r

o

z

e

Strains

Collimonas pratensis

Strain PMB3(1)

Wild type strain

t

a

/

.

,

2

0

0

7

Δ NRPS (PMB3(1)(NRPS::Gm))

Wild type strain, with Gm^R cassette inserted in double crossing over

T

h

i

s

s

t

u

d

y

Escherichia coli

DH5 α

sup E44, Δ lacU169, (Φ lacZ Δ M15), recA1, endA1, hsdR17, thi-1, gyrA96, L

relA1

a

b

c

o

l

l

e

c

t

i

o

n

L

a

b

S17.1 λ pir

TpR Sm^R recA, thi, pro, hsdRM+, RP4: 2-Tc:Mu: Km Tn7 λ pir

c

o

l

l

e

c

t

i

o

n

Plasmids

pUC1318

Amp^R, Gm^R

L

a

b

c

o

l

l

e

c

t

i

o

n

K

i

t

P

pGEM-T Easy

Amp^R

r

o

n

e

g

a

T

h

i

s

pGEM-NRPS

pGEM-T Easy carrying a NRPS fragment

s

t

u

d

y

T

h

i

s

pGEM-NRPS::Gm

pGEM-NRPS with insertion in SmaI of the Gm^R cassette

s

t

u

d

y

L

a

b

pK19mob

Km^R

c

o

l

l

e

c

t

i

o

n

pK19mob-NRPS::Gm

pK19mob containing a EcoRI fragment obtained from pGEM-NRPS::Gm

T

h

i

s

s

t

u

d

y

Primers		T _m (°C)	
For-NRPS	5'-GCCCATCCAATACGCCGATTAC-3'	54	This study
Rev-NRPS	5'-GGTCGGACCGTAGTGATTGATG-3'		This study

1035

1036


1037 **Table 2: Description of the NRPS region involved in siderophore production by *Collimonas pratensis* strain PMB3(1)**

1038 Each gene of the region of interest is presented with its NCBI accession number. Both MaGe and NCBI annotations are displayed.

1039 The putative function of each gene is indicated by a color code (regulation (purple); siderophore biogenesis (green) including NRPS

1040 (red); transport and utilization of the siderophore (blue); unknown function (grey)).

1041

Putative function	Accession number	Length (pb)	Gene	MaGe	NCBI analyses	
				Annotat ion	Annotation	% identity *
	NKI69287.1	651	<i>mbaF</i>	DNA- directed RNA polymer ase specializ ed sigma subunit,	DNA-directed RNA polymerase specialized sigma subunit, sigma24-like protein	77%

*Collimonas
fungivorans*
Ter331

				sigma24 -like protein putative MbtH- like domain putative taurine cataboli sm dioxyge nase TauD/F putative sideroph ore transpor t system ATP- binding protein YusV			
●	NKI69288.1	309	<i>mbaG</i>	putative MbtH-like domain	81%	<i>Collimonas sp.</i> MPS11E8	
●	NKI69289.1	1023	<i>mbaH</i>	putative taurine catabolism dioxygenase TauD/F	92%	<i>Collimonas sp.</i> MPS11E8	
●	NKI69290.1	876	<i>mbaI</i>	ABC cobalamin/Fe3+- siderophores transporter, ATPase subunit	81%	<i>Collimonas fungivorans</i> Ter331	

●	NKI69291.1	2094	<i>mbaJ</i>	putative iron- hydroxa mate transporter permease subunit	Fe(3+)-hydroxamate ABC transporter permease FhuB	79%	<i>Burkholderia sp.</i> K24
●	NKI69292.1	813	<i>mbaK</i>	Ferric reductase	siderophore-iron reductase FhuF	71%	<i>Collimonas sp.</i> OK412
●	NKI69293.1	1014	<i>mbaL</i>	putative iron compound ABC transporter	putative iron compound ABC transporter	86%	<i>Collimonas sp.</i> MPS11E8
●	NKI69294.1	1746	<i>mbaN</i>	ABC- type siderophore export	cyclic peptide export ABC transporter	93%	<i>Collimonas sp.</i> OK412

				system, fused ATPase and permea se compon ents			
				Non- ribosom al peptide syntheta se module putative NRPS	non-ribosomal peptide synthase domain TIGR01720/amino acid adenylation domain-containing protein		
●	NKI69295.1	9666	<i>mbaA</i>			79%	<i>Collimonas sp.</i> OK412
				amino acid adenylat ion domain	putative NRPS amino acid adenylation domain		
●	NKI69296.1	5076	<i>mbaB</i>			84%	<i>Collimonas sp.</i> MPS11E8

●	NKI69297.1	1374	<i>mbaC</i>	L-ornithine 5-monooxygenase putative TonB-dependent siderophore receptor	putative L-ornithin-5-monooxygenase	96%	<i>Collimonas sp.</i> MPS11E8
●	NKI69298.1	2220	<i>mbaD</i>	N(5)-hydroxyornithine formyltransferase, PvdF-type	putative TonB-dependent siderophore receptor, partial	96%	<i>Collimonas sp.</i> MPS11E8
●	NKI69299.1	822	<i>mbaE</i>	Isoquinoline 1-oxidoreductase	N(5)-hydroxyornithine transformylase, PvdF-type	89%	<i>Collimonas sp.</i> OK412
●	NKI69300.1	2358	<i>iorB</i>	xanthine dehydrogenase family molybdopterin-binding	xanthine dehydrogenase family protein	95%	<i>Collimonas sp.</i> PA-H2

				beta subunit Isoquino line 1- oxidored uctase subunit alpha	subunit (2Fe-2S)-binding protein	99%	<i>Collimonas sp.</i> PA-H2
●	NKI69301.1	465	<i>iorA</i>				

1042 **Figure 1: Impact of increasing concentrations of iron on chelating and growth abilities**

1043 **Siderophore activity. (A)** The *Collimonas pratensis* strain PMB3(1) WT (top) and its

1044 Δ NRPS mutant (bottom) were incubated for 3 days at 25 °C on CAS solid medium.

1045 The presence of a siderophore activity is determined by the production of yellow halo

1046 around the colony. **(B)** To determine the concentration of iron inhibiting siderophore

1047 production, liquid cultures of WT (red) and Δ NRPS (blue) were performed with

1048 different concentrations of iron (*i.e.* 0.5; 0.6; 0.7; 0.8; 0.9; 1.0 mg/l). Pure water

1049 (black) was used as a negative control. After 3 days, the absorbance at 655 nm was

1050 measured. The absorbance measured at 655 nm detects blue colour, yellow colour

1051 (corresponding to siderophore activity) will result of a decrease of the absorbance

1052 measured.

1053 **Growth assay. (C)** The growth of the WT strain (red) and Δ NRPS mutant (blue) was

1054 monitored in presence (full circle) or absence (empty circle) of EDTA (10 mM) and

1055 with iron (1 mg/l) in AB medium (2 g/l mannitol). The growth was performed under

1056 orbital shaking at 25°C for 90 h. The absorbance was measured at 600 nm every 3

1057 hours. Each dot is the mean of independent triplicates.

1058

1059 **Figure 2: Organization of the genomic region involved in the biosynthesis of**
1060 **siderophore in *Collimonas pratensis* strain PMB3(1)**

1061 Each wide arrow represents one gene and the size is according to the gene length.
1062 Gene annotation is shown under each gene and the complete description is provided
1063 in Table 2. Fine grey arrows represent promoters. Thin black arrows represent *mbaF*-
1064 dependent promoters with specific -35 and -10 regions (TAAA/n(17)/CGTC)
1065 (Thomas, 2007). The purple gene encodes a putative sigma regulation factor. Green
1066 genes are responsible for the siderophore biosynthesis and the two NRPS genes are
1067 specifically represented in red. The blue genes are involved in the siderophore
1068 utilisation and transport. The two white genes have unknown function in siderophore
1069 biosynthesis or utilisation, and represent potential accessory genes involved in
1070 siderophore production. The little red arrow in the *mbaA* gene indicates the *SmaI*
1071 restriction site used for the insertion of the gentamycin resistance cassette to create
1072 the Δ NRPS mutant.

1073

1074 **Figure 3: HPLC analysis and determination of the siderophore activity in the fractions**
1075 **collected**

1076 **(A) HPLC analysis and UV detection.** Products analysis of the pre-purified
1077 supernatant of the WT strain (red), Δ NRPS mutant (blue) and non-inoculated medium
1078 (black) were monitored at 210 nm after HPLC separation using a Milli-Q water /
1079 acetonitrile gradient for 40 min at 1 ml/min. A major peak at 1.2 min retention time
1080 and two smaller peaks at 2.2 and 3.8 min retention time were detected in the
1081 supernatant of the WT strain. These three peaks are highlighted by red arrows. **(B)**
1082 **Overlay of the HPLC and CAS analyses.** To determine the presence of a siderophore
1083 activity, fractions were collected during the HPLC run and tested using the liquid CAS
1084 assay (activity level on the right axis). The HPLC spectra of the WT strain (red line;
1085 left axis), the mutant Δ NRPS (blue line; left axis) and the medium (black line; left
1086 axis) were overlaid with the siderophore activity measured by the CAS test on the
1087 fractions for the WT strain (red dotted line; right axis), the mutant Δ NRPS (blue
1088 dotted line; right axis) and the medium (black dotted line; right axis).

1089

1090 **Figure 4: Chemical characterization of siderophore and ferrisiderophore**

1091 ESI⁺-HRMS analysis of the fraction collected at 1.2 min (after HPLC purification) from
1092 the crude extract of the WT strain was performed. **(A) Without prior incubation with**

1093 iron, the spectrum shows a major signal at $m/z = 623.3069$ (mono-protonated ion
1094 $[M+H]^+$) which indicates a siderophore exact mass of $M_S = 622.3069$. **(B) After prior**
1095 **incubation with iron**, the analysis reveals a major signal at $m/z = 676.2191$ (mono-
1096 protonated ion $[M+H]^+$) which indicates a ferrosiderophore exact mass of $M_{FS} =$
1097 675.2191 . The isotopic pattern detailed in the dashed inset shows the obvious
1098 presence of an iron atom in the structure, thanks to the clear contributions of ^{54}Fe
1099 and ^{56}Fe (*i.e.*, $m/z = 674.2246$ with 5.7 % ratio and $m/z = 676.2191$ respectively). **(C)**
1100 **MS/MS spectrum.** The previously highlighted siderophore compound ($MS =$
1101 622.3069) was further analyzed by ESI-MS/MS to validate its structure. M/z values
1102 framed in red correspond to theoretical fragments consecutive to breaking of the
1103 peptide bonds of the expected siderophore (m/z values framed in orange correspond
1104 to the dehydrated forms). **(D) Theoretical structure and fragmentation of malleobactin**
1105 **X.** Each letter represents the amino acid letter code forming the malleobactin X. The
1106 cleavage of the different peptide bonds (blue dashed lines) results in the formation of
1107 different ions containing the N-terminus of the peptide (b) and to ions containing the
1108 C-terminus of the peptide (y). Depending on the peptide bond cleaved, different
1109 fragments can be formed and their mass is presented as $b(1,2,3,4)$ and $y(1,2,3,4)$.

1110 The fragments identified experimentally (see panel C), which mass corresponds to
1111 the theoretical masses, are presented in red, the other are presented in blue. (E)
1112 **Structure and composition of the malleobactin X.** The molecule represented
1113 corresponds to the reference malleobactin X predicted by Vargas-Straube et al.
1114 2016. The name of each amino acid is written in full under the molecule as well as its
1115 one letter abbreviation.

1116

1117 **Figure 5: Phylogenetic tree based on the NRPS MbaA protein**

1118 The conservation of the protein MbaA among *Collimonas* and other related genera
1119 (*Paraburkholderia*, *Burkholderia*, *Caballeronia*, *Herbaspirillum*) is presented on this
1120 phylogenetic tree. A set of 52 NRPS protein sequences was analyzed and is detailed
1121 in the Table S1. Our model strain *Collimonas pratensis* PMB3(1) is in bold. The
1122 distribution and relatedness to known NRPS types is indicated by a color code:
1123 ornibactin (*i.e.* Orbl-like protein: green circles), malleobactin (*i.e.* MbaA-like protein;
1124 red circles) or serobactin (purple circles). The MbaA homologues for which
1125 production of such siderophore was experimentally demonstrated or only predicted
1126 are presented with full circles and empty circles, respectively. The production of

1127 ornibactin have been experimentally demonstrated for 3 strains included in the
1128 analysis (full green circle; (Meyer *et al.*, 1995; Darling *et al.*, 1998; Deng *et al.*, 2017).
1129 Malleobactin was identified in three strains included in the analysis (full red circle;
1130 (Alice *et al.*, 2006; Franke *et al.*, 2013; Vargas-Straube *et al.*, 2016). The other proteins
1131 considered in this analysis had only predicted function (empty circle; (Holden *et al.*,
1132 2009; Schwager *et al.*, 2013; Song *et al.*, 2015; Esmael *et al.*, 2016, 2018). The
1133 siderophores predicted as ornibactin and discussed in this study are represented by
1134 green dotted circles. Letters inside circles correspond to the cited reference (in the
1135 figure) in which the prediction or demonstration was/were done.

1136

1137 **Figure 6: Determination of the weathering ability of the WT *Collimonas pratensis***
1138 **strain PMB3(1) and its Δ NRPS mutant**

1139 The hematite weathering potential of strain PMB3(1) and its Δ NRPS mutant was
1140 evaluated by the measure of iron released from hematite in ABm medium devoid of
1141 iron, after 7 days of incubation at 25°C under agitation (200 rpm). Non-inoculated
1142 media with and without hematite (termed Hematite and Medium respectively) were
1143 used as control. **(A) Quantity of iron released in solution.** The iron released from

1144 hematite was measured by ferrospectral determination (optical density measured at
1145 595nm). A standard calibration of iron (FeCl_3) was used to calculate the iron
1146 concentration of the different samples tested (WT, ΔNRPS , hematite alone or
1147 Medium alone). Samples with the same letter indicate no significant difference
1148 ($P < 0.05$). **(B) pH of the supernatant.** The acidification of the medium was measured
1149 by absorbance at 595nm using the bromocresol green method. **(C) Siderophore**
1150 **activity.** The siderophore activity of the different samples was determined using the
1151 CAS method. The yellow colour indicates a siderophore activity. For each measure,
1152 data are presented under the corresponding pictures and are the mean of
1153 independent triplicates, the standard deviation is indicated in *italic*.